Available online at www.sciencedirect.com
ScienceDirect
Journal of Catalysis 251 (2007) 233–238
JOURNAL OF CATALYSIS
www.elsevier.com/locate/jcat

Reserach Note

Highly active mesoporous Co–B amorphous alloy catalyst for cinnamaldehyde hydrogenation to cinnamyl alcohol

Hui Li, Haixia Yang, Hexing Li *

Department of Chemistry, Shanghai Normal University, Shanghai 200234, PR China

Received 28 April 2007; revised 12 July 2007; accepted 12 July 2007

Available online 28 August 2007

Abstract

A novel mesoporous Co–B amorphous alloy was synthesized by controlling the chemical reduction of Co^{2+} with BH_4^- in the presence of surfactant. During liquid-phase cinnamaldehyde hydrogenation, mesoporous Co–B exhibited higher activity and selectivity to cinnamyl alcohol compared with nonporous Co–B. This higher activity was attributed to its high surface area and mesopores, which facilitated diffusion and adsorption of reactants, whereas its better selectivity was ascribed to the uniform distribution of Co active sites and their connection via a porous network, which facilitated the competitive hydrogenation of C=O against C=C coexisting in the cinnamaldehyde molecule, because C=C adsorption was inhibited due to steric hindrance.

Keywords: Co–B amorphous alloy catalyst; Mesoporous structure; Surfactant self-assembly; Cinnamaldehyde; Hydrogenation; Cinnamyl alcohol

1. Introduction

Amorphous alloy catalysts are of considerable interest due to their potential in industrial catalysis [1–3]. Since the 1980s, numerous amorphous alloy catalysts have been synthesized by chemical reduction and their catalytic performance has been widely investigated [4–7]. However, the effect of catalyst shape has not received much attention until recently, because nearly all of the amorphous alloy catalysts are present in the form of nonporous nanoparticles. Recently, Zhu et al. [8] reported a synthesis route to prepare amorphous catalysts with nanotube structure via surfactant self-assembly. Obviously, mesoporous amorphous alloys represent a new trend toward the design of highly active catalysts with high surface area and large pore channels that favor both adsorption and diffusion of reactants [9–13]. However, preparation of mesoporous amorphous alloys is difficult, because the surfactant-templated mesoporous structure in liquid crystalline phases is usually damaged by the vigorous and strongly exothermic reaction between metallic ions and reducing agents [14]. Previously, we reported that Co–B amorphous alloy was highly selective to cinnamyl alcohol (CMO) during liquid-phase cinnamaldehyde (CMA) [15,16]; however, this Co–B catalyst showed poor activity due to its low surface area. Because the Co–B catalyst prepared by traditional methods is nonporous, the particle size should be controlled to be as small as possible to achieve high activity, which might induce problems in separation and also cause agglomeration. Here we report a mesoporous Co–B amorphous alloy catalyst with enhanced activity and selectivity to CMO in CMA hydrogenation obtained via surfactant self-assembly.

2. Experimental

The mesoporous Co–B amorphous alloy was synthesized according to the following procedure. At 308 K, 7.3 ml of 3.0 M KBH_4 aqueous solution was added dropwise to a homogeneous solution comprising 45 ml of ethanol (EtOH, 99.98%) and 20 ml of aqueous solution containing 2.0 g of hexadecyltrimethyl-ammonium bromide (CTAB), 3.0 g of $Co(CH_3COO)_2$ (i.e., 1.0 g Co), and a trace amount of antifoaming agent. After complete reduction of Co^{2+} in the solution, the black solid was washed free from inorganic ions and soluble organic substances with H_2O, followed by extraction in 1000 ml of EtOH for 14 h

* Corresponding author. Fax: +86 21 64322272.
E-mail address: hexing-li@shnu.edu.cn (H. Li).

0021-9517/$ – see front matter
doi:10.1016/j.jcat.2007.07.022

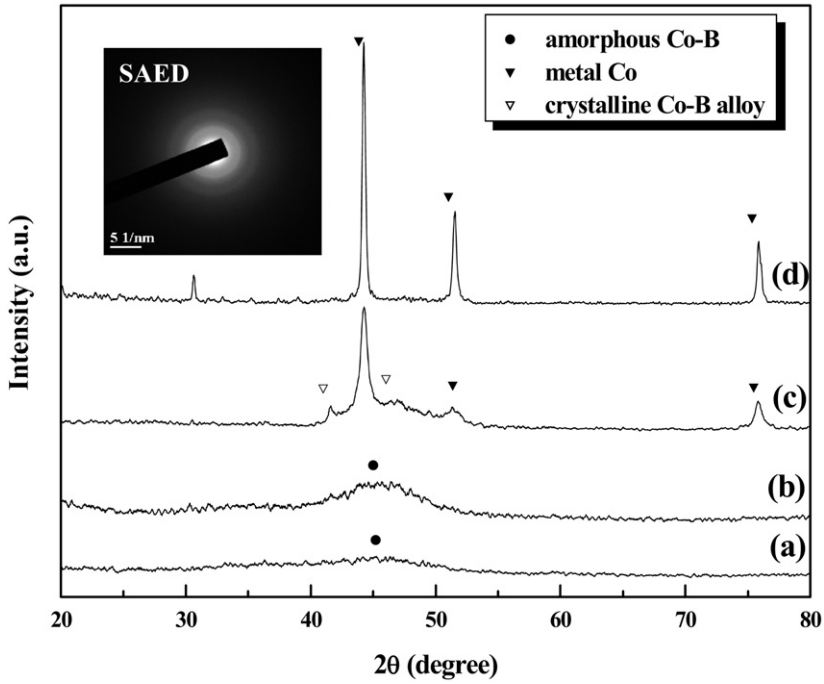

Fig. 1. Wide-angle XRD patterns of the Co–B samples treated at different temperatures in N_2 flow for 2 h: (a) as-received, (b) 473 K, (c) 673 K and (d) 873 K. The insert is the SAED image of the fresh Co–B sample.

at 353 K. For comparison, nonporous Co–B amorphous alloy also was prepared by the traditional method [15].

Catalysts were characterized by inductively coupled plasma optical emission spectrometry (ICP), X-ray powder diffraction (XRD), Fourier transform infrared (FTIR) spectroscopy, N_2 adsorption–desorption, transmission electron microscopy (TEM), selected area electronic diffraction (SAED), X-ray photoelectron spectroscopy (XPS), H_2 chemisorption, and H_2 temperature-programmed desorption (H_2-TPD). Before TEM measurement, the sample was ultrasonically dispersed in ethanol and supported on carbon-coated copper grids.

Liquid-phase hydrogenation of CMA was carried out at 373 K and 1.0 MPa H_2 in a stainless steel autoclave containing a catalyst with 0.25 g of Co, 45 ml of EtOH, and 3.0 ml of CMA. The initial specific activity (R_H^m = mmol/(h g Co)) and areal activity (R_H^S = mmol/(h m^2 Co)) were calculated based on the pressure drop within the first 30 min. To obtain conversion and selectivity, the reaction mixture was sampled every 30 min for product analysis on a gas chromatograph (GC 102) with a flame ionization detector and a 15% Apiezon (L)/Gas Chrom (red) column at 423 K with N_2 flow as a carrier gas. The reproducibility of the results was checked by repeating the runs at least three times; the results were found to be within acceptable limits (±5%).

3. Results and discussion

FTIR spectra demonstrated that surfactant in the as-prepared Co–B sample was completely removed, because no significant absorbance peaks indicative of CTAB molecule at 2918, 2852, 1554, and 960 cm^{-1} [17] could be observed after extraction in EtOH. XPS spectra revealed that all of the Co species in Co–B sample were present in metallic state, corresponding to binding energy (BE) of ca. 778.3 eV. But the B species were present in two states, elemental B and oxidized B (B_2O_3), corresponding to a BE of 187.8 and 192.1 eV, respectively. The BE of elemental B in the Co–B sample was 0.7 eV higher than that of pure B, indicating that the elemental B was not present in the free state but instead was alloying with the metallic Co, in which partial electrons transfer from B to Co [7]. A wide-angle XRD pattern (Fig. 1) demonstrated the amorphous structure, with only one broad peak at ca. $2\theta = 45°$ observed in the fresh Co–B sample [18]. Treatment of the fresh Co–B at elevated temperatures from 573 to 873 K in N_2 atmosphere for 2 h resulted in gradual disappearance of the original broad peak and appearance of diffraction peaks corresponding to crystalline Co–B alloy and metallic Co, indicating the transformation from an amorphous structure to a crystalline structure, along with decomposition of Co–B amorphous alloy. During the crystallization process, the appearance of Co–B crystalline phases further verified the formation of an alloy between Co and B for mesoporous Co–B. Thus, combining the results from XRD and XPS characterizations can demonstrate formation of the Co–B amorphous alloy. This can be further confirmed by the SAED image, in which a series of successive diffraction halos characteristic of amorphous alloys can be seen [19].

The small-angle XRD pattern of the fresh Co–B (Fig. 2) displays a well-resolved diffraction peak indicative of mesoporous structure around $2\theta = 0.68°$. The lower peak intensity and the absence of additional small peaks at larger 2θ implies the poor ordering degree of the mesoporous structure, which is confirmed by the TEM image, in which only a worm-like porous structure can be seen in the as-prepared Co–B sample. Meanwhile, the N_2 adsorption–desorption isotherm also dis-

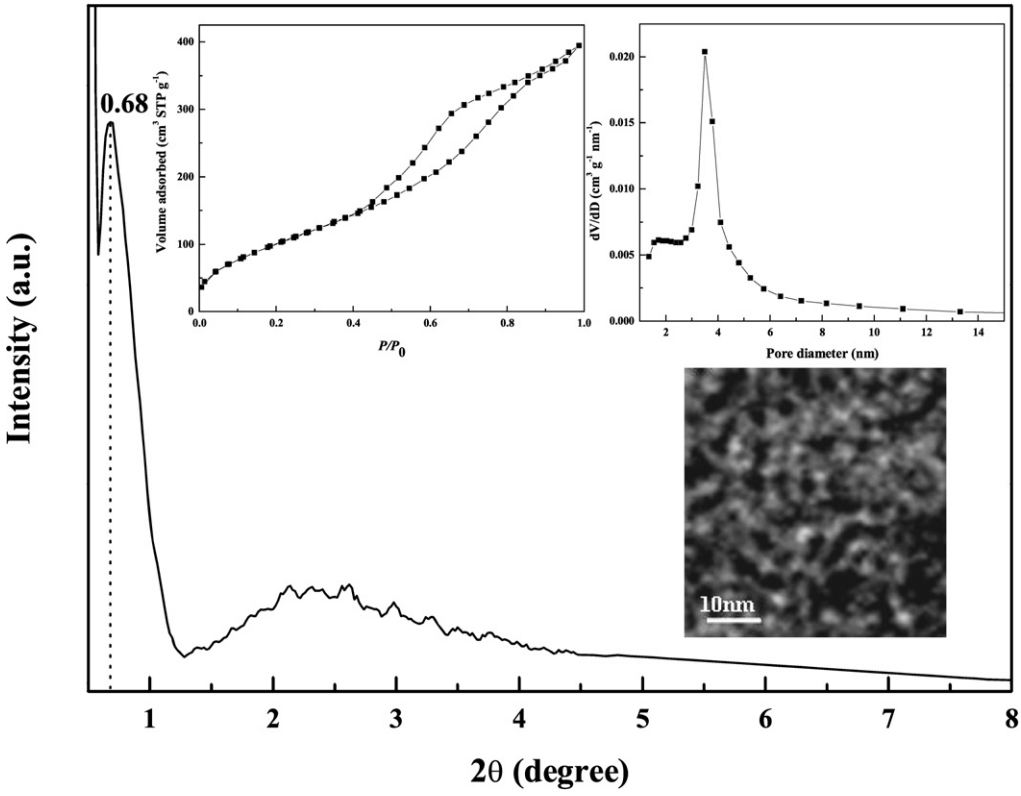

Fig. 2. Small-angle XRD pattern of the fresh Co–B sample. Inset: N_2 adsorption–desorption isotherm, BJH pore size distribution curve and TEM image of the fresh Co–B sample.

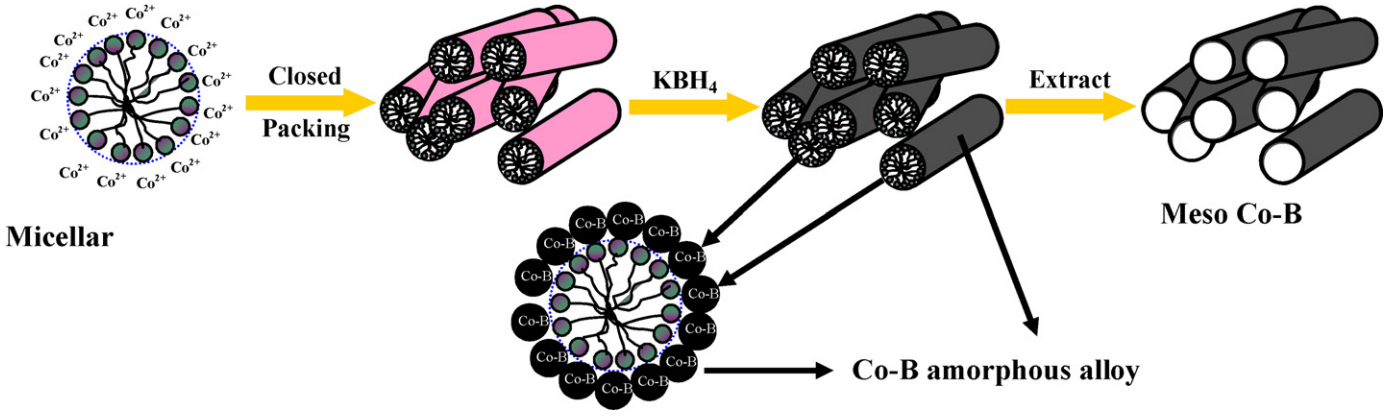

Scheme 1. Schematic illustration of the formation of mesoporous structure in Co–B amorphous alloy particles.

plays a H_1 hysteresis indicative of mesoporous structure in the as-prepared Co–B sample [20]. The BJH pore size distribution demonstrated a relatively uniform porous structure centered at 3.8 nm. The mesoporous structure in Co–B sample could be preserved after treatment in N_2 flow at 473 K for 2 h or in ethanol solution at 373 K for 12 h; however, further increases in treatment temperature resulted in collapse of the mesoporous structure.

The formation of mesoporous Co–B can be simply described in Scheme 1. Surfactant self-assembly in the water–alcohol mixing solvent generates a micellar structure, which further aggregates into liquid crystalline mesophases at high concentration [21]. Co^{2+} ions can co-assemble with CTAB to form nanocomposites containing ordered surfactant lyotropic liquid crystalline phases. Chemical reduction of these Co^{2+} ions by KBH_4 produces Co–B amorphous alloy covering the liquid crystalline mesophases via –Co–Co– and/or –Co–B–Co–B– bonding and constructs the mesopore walls in the Co–B amorphous alloy after extraction of the surfactant [22]. No mesoporous Co–B could be obtained in the absence of the antifoaming agent or when $CoCl_2$ was used instead of $Co(CH_3COO)_2$, due to the vigorous and strongly exothermic reaction between Co^{2+} and BH_4^-, which destroys the ordered mesostructure in the liquid crystalline phase. The reduction of $Co(CH_3COO)_2$ by KBH_4 proceeds smoothly due to the coordination of CH_3COO^- with Co^{2+}; however, only a worm-

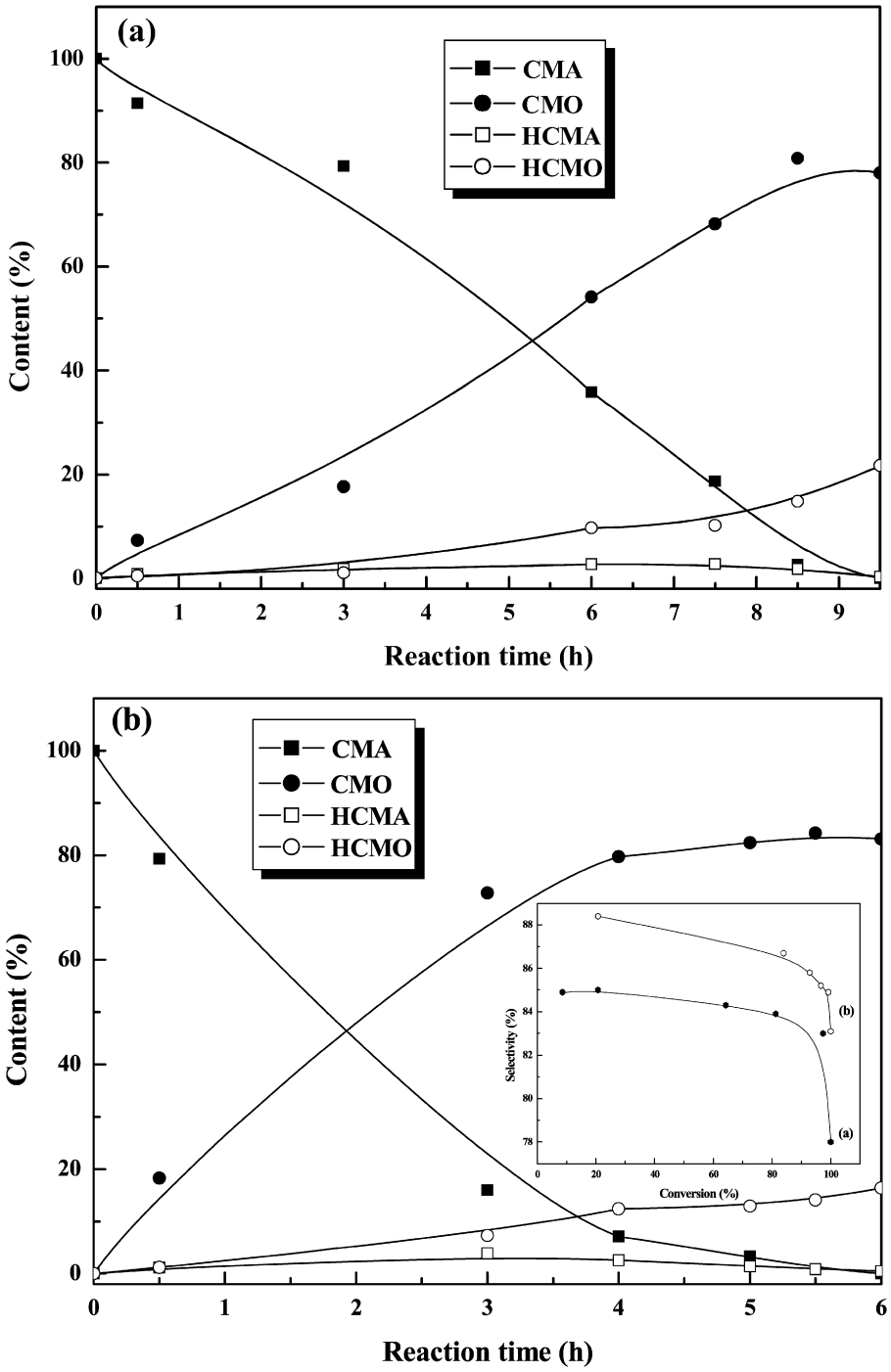

Fig. 3. Reaction profiles of CMA hydrogenation over (a) nonporous Co–B and (b) mesoporous Co–B amorphous alloy catalysts. The insert is the dependency of selectivity to CMO on CMA conversion during CMA hydrogenation over (a) nonporous Co–B and (b) mesoporous Co–B amorphous alloy catalysts.

like mesoporous structure with poor ordering degree could be formed.

The catalytic performance of mesoporous Co–B was evaluated and compared with that of other catalysts using CMA hydrogenation as a probe; this important reaction is widely used in the production of perfumes, flavorings, pharmaceuticals, and other fine chemicals [23]. The reaction profiles of CMA hydrogenation (Fig. 3) demonstrated the formation of both CMO and dihydrocinnamaldehyde (HCMA), obviously due to the competitive hydrogenation between C=C and C=O coexisting in the CMA molecule. In addition, 3-phenylpropanol (HCMO) also was detected, which can be attributed to the further hydrogenation of either CMO or HCMA [23]. Table 1 summarizes the catalytic parameters of different Co-based catalysts. Both mesoporous Co–B and nonporous Co–B exhibited much higher activity and selectivity to CMO compared with Raney Co, which can be attributed to the promoting effects from both the unique amorphous structure and the electronic interaction

Table 1
Structural and catalytic parameters of the Co–B amorphous catalysts[a]

Sample	Comp. (at%)	Surf. comp. (at%)	S_{Co} (m^2/g)	R_H^m (mmol/(h g Co))	R_H^S (mmol/(h m^2 Co))	Time[b] (h)	Yield[c] (%)
Raney Co	Co	/	30.9	10.1	0.33	9.0	66.2
Mesoporous Co–B	$Co_{67.4}B_{32.6}$	$Co_{71.7}B_{28.3}$	27.7	28.1	1.01	5.5	84.2
Nonporous Co–B	$Co_{64.0}B_{36.0}$	$Co_{72.0}B_{28.0}$	12.2	11.8	0.97	8.5	80.8
Crystalline Co–B-1[d]	$Co_{64.0}B_{36.0}$	/	7.1	4.9	0.69	15	72.3
Crystalline Co–B-2[e]	$Co_{67.4}B_{32.6}$	/	9.0	5.8	0.64	12.5	73.5

[a] Reaction conditions: the catalyst containing 0.25 g Co, 3.0 ml of CMA, 45 ml of EtOH, 1.0 MPa H_2, 373 K.
[b] Reaction time needed to reach maximum CMO yield.
[c] Maximum CMO yield.
[d] Obtained by treating the fresh nonporous Co–B sample at 873 K for 2 h in N_2 flow.
[e] Obtained by treating the fresh mesoporous Co–B sample at 873 K for 2 h in N_2 flow.

between metallic Co and alloying B [7]. The R_H^m values indicate that mesoporous Co–B was more active than nonporous Co–B, whereas the similar R_H^S values imply that they exhibited similar intrinsic activities, which can be attributed to their similar compositions, amorphous alloy structures, and surface electronic characteristics. Thus, the higher activity of mesoporous Co–B can be attributed mainly to its higher active surface area (S_{Co}) due to the mesoporous structure. The dependence of CMO selectivity on CMA conversion during CMA hydrogenation (Fig. 3b) reveals that mesoporous Co–B was also slightly more selective to CMO than nonporous Co–B. The TEM morphologies demonstrate Co–B particles interconnected via a porous network. Such conjugated Co active sites could reduce the adsorption of the C=C bond in the CMA molecule due to the steric hindrance from the neighboring benzene ring connecting with C=C [24], which may inhibit C=C hydrogenation, leading to higher CMO selectivity. The uniform distribution of Co active sites in the mesoporous network is another important factor contributing to the higher selectivity. According to the H_2-TPD results, mesoporous Co–B displayed an intense hydrogen desorption peak at 753.5 K and a small shoulder peak at 680.8 K, whereas nonporous Co–B exhibited three peaks at around 697.7, 784.8 and 893.3 K, respectively. The lower number of desorption peaks and the narrower temperature range corresponding to hydrogen desorption suggest that mesoporous Co–B contains relatively uniform Co active sites, which may favor the selectivity in CMA hydrogenation. Meanwhile, mesoporous Co–B exhibited stronger adsorption for hydrogen than nonporous Co–B, due to the synergistic effect of conjugated Co active sites. The hydrogen atoms strongly adsorbed on Co active sites are favorable for the competitive hydrogenation of C=O against C=C coexisting in CMA [25], leading to higher CMO selectivity. Treatment of either mesoporous Co–B or nonporous Co–B at 873 K for 2 h in N_2 flow led to abrupt decrease in activity and selectivity; obviously due to the crystallization of Co–B amorphous alloy and decrease in S_{Co} (see Table 1).

4. Conclusion

In summary, the present work outlines a new approach to designing a Co–B amorphous alloy catalyst with mesoporous structure by a surfactant-templating method. Such a Co–B catalyst exhibits much higher activity and even better selectivity to CMO compared with the nonporous Co–B obtained by the traditional method of CMA hydrogenation, apparently due to its high active surface area and mesoporous channels, which facilitate adsorption and diffusion of reactant molecules. Using the present method, more metal–boron amorphous alloys can be prepared by controlling the rate of reaction between metallic ions and KBH_4, which will offer new opportunities for industrial applications.

Acknowledgments

This work was supported by the National Natural Science Foundation of China (20603023), the Preliminary 973 Project (2005CCA01100), and the Shanghai Government (05QMX 1442, 0552nm036, T0402, 05DZ20, 06JC14060, 06JC14093).

References

[1] Y. Chen, Catal. Today 44 (1998) 3.
[2] J.F. Deng, J. Yang, S.S. Sheng, J. Catal. 150 (1994) 434.
[3] A. Baiker, Faraday Discuss. Chem. Soc. 87 (1989) 239.
[4] J.A. Schwarz, C. Contescu, A. Contescu, Chem. Rev. 95 (1995) 477.
[5] J. van Wonterghem, S. Mørup, C.J.W. Koch, S.W. Charles, S. Wells, Nature 322 (1986) 622.
[6] H.X. Li, W.J. Wang, J.F. Deng, J. Catal. 191 (2000) 257.
[7] H.X. Li, Y.D. Wu, H.S. Luo, M.H. Wang, Y.P. Xu, J. Catal. 214 (2003) 15.
[8] Y. Zhu, F.P. Liu, W.P. Ding, X.F. Guo, Y. Chen, Ang. Chem. Int. Ed. 45 (2006) 7211.
[9] C.T. Kresge, M.E. Leonowicz, W.J. Roth, J.C. Vartuli, J.S. Beck, Nature 359 (1992) 710.
[10] G.S. Attard, C.G. Göltner, J.M. Corker, S. Henke, R.H. Templer, Angew. Chem. Int. Ed. 36 (1997) 1315.
[11] D.Y. Zhao, J. Feng, Q. Huo, N. Melosh, G.H. Fredrickson, B.F. Chmelka, G.D. Stucky, Science 279 (1998) 548.
[12] F. Bouchama, M.B. Thathagar, G. Rothenberg, D.H. Turkenburg, E. Eiser, Langmuir 20 (2004) 477.
[13] H.X. Li, Q.F. Zhao, Y. Wan, W.L. Dai, M.H. Qiao, J. Catal. 244 (2006) 251.
[14] Y. Yamauchi, T. Yokoshima, T. Momma, T. Osaka, K. Kuroda, J. Mater. Chem. 14 (2004) 2935.
[15] H.X. Li, X.F. Chen, Y.P. Xu, Appl. Catal. A 225 (2002) 117.
[16] H.X. Li, H. Li, J. Zhang, W.L. Dai, M.H. Qiao, J. Catal. 246 (2007) 301.
[17] A.S.M. Chong, X.S. Zhao, J. Phys. Chem. B 107 (2003) 12650.
[18] A. Yokoyama, H. Komiyama, H. Inoue, T. Masumoto, H.M. Kimura, J. Catal. 68 (1981) 355.
[19] K.S. Martens, J.A. Parton, R. Vercruysse, K. Jacobs, P.A. Maier, Catal. Lett. 38 (1996) 209.
[20] Y. Lu, H. Fan, A. Stump, T.L. Ward, C.J. Brinker, Nature 398 (1999) 223.

[21] J.S. Beck, J.C. Vartuli, W.J. Roth, M.E. Leonowicz, C.T. Kresge, K.D. Schmitt, C.T.-W. Chu, D.H. Olson, E.W. Sheppard, S.B. McCullen, J.B. Higgins, J.L. Schlenkert, J. Am. Chem. Soc. 114 (1992) 10834.
[22] B.R. Shen, S.Q. Wei, K.N. Fan, J.F. Deng, Appl. Phys. A 65 (1997) 295.
[23] T.B.L. Marinelli, M.S. Nabuurs, V. Ponec, J. Catal. 151 (1995) 431.
[24] T.B.L.M. Marinelli, V. Ponec, J. Catal. 156 (1995) 51.
[25] H.R. Hu, M.H. Qiao, S. Wang, K.N. Fan, H.X. Li, B.N. Zong, X.X. Zhang, J. Catal. 221 (2004) 612.